Engineering Structures 296 (2023) 116913

Contents lists available at ScienceDirect

Engineering Structures

journal homepage: www.elsevier.com/locate/engstruct

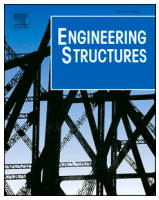

Bridge frequency identification in city bus monitoring: A coherence-PPI algorithm

Yifu Lan [a], Zhenkun Li [a], Keijo Koski [b], Ludovic Fülöp [b], Timo Tirkkonen [c], Weiwei Lin [a,*]

[a] Department of Civil Engineering, Aalto University, 02150 Espoo, Finland
[b] VTT Technical Research Center of Finland Ltd., P.O. Box 1000, FI-02044 Espoo, Finland
[c] The Finnish Transport Infrastructure Agency (FTIA), P.O. Box 33, 00521 Helsinki, Finland

ARTICLE INFO

Keywords:
Drive-by bridge inspection
City bus
Bayesian framework
Bridge frequency identification
Vehicle-bridge interaction
Monte Carlo method

ABSTRACT

Recently, drive-by-bridge inspection methods have attracted substantial scholarly interest; however, their practical implementation has encountered significant challenges. In engineering practice, even simply extracting bridge frequencies from ordinary or commercial vehicles appears to be difficult; components related to factors such as road roughness often dominate vehicle vibration responses. This study proposes a novel coherence-PPI (Prominent Peak Identification) algorithm based on the Bayesian framework and applies it to city bus bridge monitoring to extract bridge frequencies. The fundamental idea is to recognize the bridge frequency as a common vibration component across various vehicle runs. The algorithm comprises the following three steps: First, coherences were computed for all vehicle runs to interpret the signal relationships. Second, a Bayesian framework was established to statistically determine the threshold that can maximize the occurrence of bridge frequency. Third, the prominent peaks (PPs) were selected based on the threshold, and their distribution was counted to identify the fundamental frequency of the bridge. In contrast to the previous studies that focused on avoiding differences (e.g., by trying to reduce variation, driving in the same lane, and using the same speed), this methodology encourages the introduction of variability in drive-by measurements to filter bridge frequencies, rendering it particularly compelling for practical engineering applications. The proposed methodology was validated through numerical studies, including the Monte Carlo method, and field tests using city buses. The results demonstrated that the method can effectively eliminate the effects of road roughness, environmental noise, and vehicle parameter variations and accurately identify the bridge frequency.

1. Introduction

Bridge frequencies represent a fundamental aspect of bridges, offering insights into critical bridge behaviors such as bearing conditions and the characterization of resonance phenomena under periodic loading [1]. Measuring frequencies is crucial for bridge health monitoring and bridge seismic design [2]; however, the conventional method of measuring bridge frequencies using sensors mounted on bridges faces several challenges. These challenges include high labor expenses, potential hazards associated with on-site installation, traffic disturbances, and maintenance costs for sensors [3]. This leads to high costs and significant delays in implementing bridge health monitoring systems for many bridges [4]. A promising alternative to conventional approaches is the drive-by bridge inspection method, which has recently gained popularity as an active area of research. This method leverages vehicles as mobile sensors to extract dynamic bridge information through a vehicle-bridge interaction (VBI) process [5]. As vehicles travel over a bridge, the resulting vibrations reflect the dynamic properties of the bridge in response [6,7]. This approach requires minimal instrumentation on the vehicle and offers a potential solution to acquire key bridge information efficiently and economically [8].

Implementing a drive-by approach within public transit systems for routine monitoring of bridges represents a prominent area of interest in the field [9,10]. For instance, if city buses that operate on a daily basis can be effectively utilized to inspect bridges in major urban areas, this can lead to efficient resource usage and significant cost reduction in monitoring, making it an ideal objective for the application of drive-by inspection methods [11]. This is particularly important for the monitoring of short- and medium-span bridges. However, in practice, it is difficult to extract bridge frequencies from buses. Currently, most

* Corresponding author.
E-mail address: weiwei.lin@aalto.fi (W. Lin).

https://doi.org/10.1016/j.engstruct.2023.116913
Received 24 May 2023; Received in revised form 18 August 2023; Accepted 17 September 2023

studies on drive-by monitoring focus on developing and verifying methodologies in numerical studies, controlled laboratory environments, and small-scale structures using specialized vehicles [12]. Drive-by measurements using ordinary vehicles on normal bridge structures are prone to large uncertainties. The amplitude of the spectral peak associated with the bridge frequency can be low, and interference signals caused by roughness components or vehicle dynamics may obscure the signal of interest [13]. Non-bridge frequency peaks are often combined with a weak bridge frequency peak (or a complete lack thereof), which can lead to misleading frequency identification [1]. Therefore, the identification of bridge information from the complex and varied signal components in vehicle responses is a critical issue in the application of drive-by methods.

In this regard, many efforts have been made in previous studies to eliminate the vibration components of the interference and extract the bridge frequency from the vehicle response. For example, Yang et al. [15] proposed the utilization of the contact point (CP) response between a bridge and a vehicle for measuring the bridge frequency; furthermore, it was discovered to be unrelated to vehicle frequency. The effect of roughness can be eliminated by subtracting the CP responses of two adjacent axles or trailers, and the bridge frequency can be identified from the resulting residual response [14,15]. However, in engineering applications, such methods may require adjacent axles/trailers to follow the same trajectory, and use special vehicles and sometimes shakers [14–17]. These are not always available in practice, and their application in buses or other ordinary/commercial vehicles for daily monitoring purposes is even more difficult.

An alternative approach involves the application of cross-spectral estimation. Nagayama et al. [1] utilized a cross-spectral density function estimation technique to extract bridge frequency as a common vibration component among the responses of two moving vehicles. The effectiveness of this method was verified through field tests. Lan et al. [18,19] experimentally obtained the bridge frequency as a signal commonality across various sensors mounted on an ordinary truck. In the cross spectrum obtained using these methods, the peaks unrelated to the bridge frequencies were weakened. However, their performance is influenced by factors such as speed, road roughness, and vehicle weight, and they do not always succeed. The multi-vehicle or multi-sensor approach used in these studies is sometimes inconvenient or costly for real-world operations (e.g., passing two or more equipped buses simultaneously on a short-span bridge may be inconvenient or even impossible). Importantly, these methodologies cannot be applied to the vast amount of existing data collected from single sensors on individual vehicles, leading to a significant underutilization of the available data resources. Nevertheless, the performance of these methods on buses in daily operation within public transportation systems remains an area worth exploring.

Bridge frequencies, as common vibrational components, can manifest across different runs of a vehicle, whereas the vibration components related to road roughness and vehicle dynamics among different vehicle passages tend to differ. Typically, it is difficult for vehicles to follow the same trajectory across bridges in different runs; therefore, the road roughness traverses and the vehicle vibrations caused by it are different. Because of factors such as speed variation, the vibration components related to vehicle dynamics (including engine vibrations) are also likely to differ. Furthermore, environmental noise, another contributor to vehicle vibrations, possesses random characteristics. Based on this, an algorithm can be developed to extract signal commonalities (i.e., bridge frequencies) from multiple runs of buses (but not limited to buses). Cross-spectral estimation forms the foundation of this algorithm, with its primary function being to weaken peaks unrelated to bridge frequencies. However, this method can only be applied to a pair of signals. The crux of the algorithm design involves rationally calculating the correlations among a large number of signal inputs and subsequently devising strategies to extract the bridge frequencies from them. It does not impose stringent requirements on vehicle parameters (such as weight and speed) or road conditions, thereby enabling routine bridge monitoring by using ordinary vehicles. The proposed algorithm represents a significant step towards the commercial or industrial implementation of drive-by methods, which is also the primary motivation behind the present work.

This study proposes a novel coherence-PPI algorithm based on the Bayesian Framework and applies it to city bus bridge monitoring to extract bridge frequencies. It consists of three processes: (1) coherence computation, (2) threshold determination, and (3) selection of PPs for frequency identification. The underlying idea is to recognize the bridge frequency as a common vibration component across various vehicle runs. To validate the proposed algorithm, numerical studies and field tests are conducted. First, a VBI model for the bus rear axle system was established, and numerical studies, including Monte Carlo methods, were conducted to investigate the effectiveness and robustness of the proposed method under various conditions (e.g., road roughness, environmental noise, and vehicle parameter variation). Subsequently, the feasibility of the proposed method in engineering practice was verified based on the results of field tests performed on the Olari and Matti bridges in Finland using city buses.

The remainder of this paper is organized as follows: Section 2 describes the three-step coherence-PPI algorithm for bridge frequency identification. Section 3 establishes a VBI model based on the rear-axle system of a bus and numerically examines the performance of the proposed algorithm under various scenarios. Section 4 describes the field tests using urban buses and their results, demonstrating the practical effectiveness of the proposed algorithm. Finally, Section 5 concludes the paper.

2. Bridge frequency identification algorithm

The proposed algorithm consists of three steps for identifying bridge frequency using the responses of a vehicle from multiple runs: (1) the coherences are calculated from all the combinations of vehicle runs to interpret the relationship between the signals. (2) A Bayesian framework is established to statistically determine the threshold. (3) The PPs are selected based on the threshold, and their distribution is counted to identify the fundamental frequency of the bridge. The fundamental idea is to identify the bridge frequency as a common vibration component among different vehicle runs.

2.1. Step 1: Coherence computation

This section presents the calculation strategy for coherence in multiple-vehicle runs. Typically, there are four main contributors to vehicle vibration: bridge vibration, road roughness, vehicle dynamics, and environmental noise [1,19]. In the frequency spectrum, the peaks associated with bridge vibration are usually not prominent when compared to others. Yet, to some extent, they are deemed to exhibit a commonality across different vehicle runs. Peaks related to road roughness and vehicle dynamics tend to vary with different trajectory, speed, etc. Environmental noise is random. This inspires the use of coherence, which is a measure used to compare the relationship between two signals, to tackle the problem [20]. The coherence between the two signals is mathematically expressed as:

$$C_{xy}(f) = \frac{\left|G_{xy}(f)\right|^2}{G_{xx}(f)G_{yy}(f)} \tag{1}$$

where $G_{xy}(f)$ is the cross-spectral density of signals x and y, $G_{xx}(f)$ is the power spectral density of signal x, and $G_{yy}(f)$ is the power spectral density of signal y.

For a vehicle traveling on the same bridge multiple times, the coherences are computed for all possible combinations of vehicle runs (see Fig. 1). If a car travels n times, then the total number of coherences is $N = C_n^2$. This represents the computation of the combinations that can be

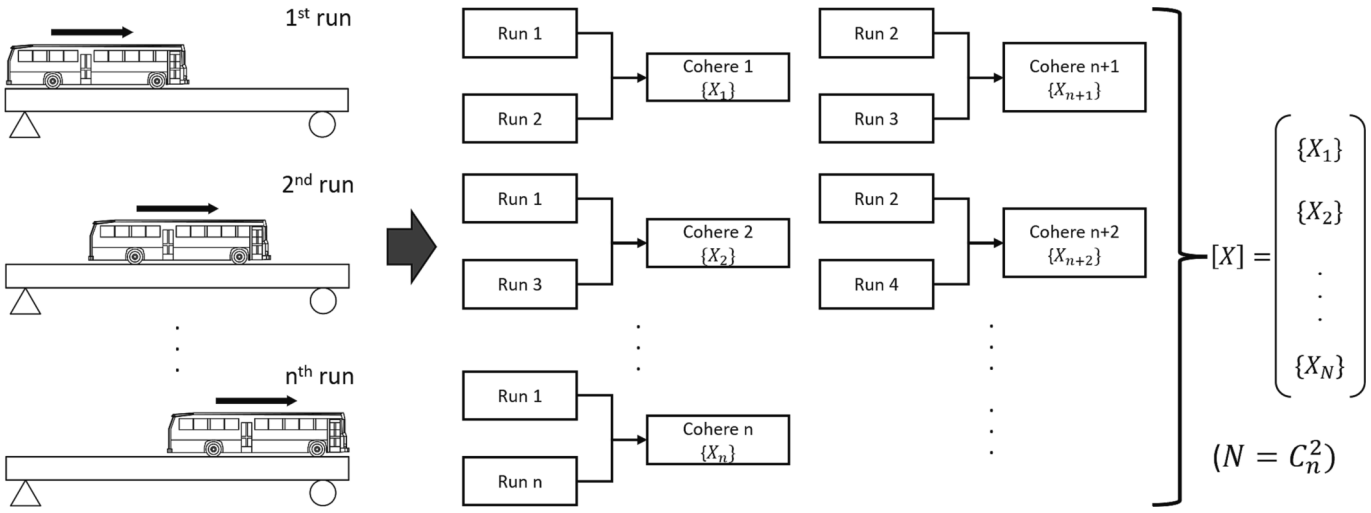

Fig. 1. Coherence computation process.

calculated using Eq. (2). The coherence of the two vehicle runs, $\{X_i\}$, is calculated using Eq. (1), which is a vector, and $[X]$ is a matrix composed of N coherence vectors.

$$C_n^2 = \frac{n!}{2(n-2)!} = \frac{n(n-1)}{2} \tag{2}$$

2.2. Step 2: Threshold determination

This section aims to determine the threshold that maximizes the occurrence of bridge-related frequencies. The Bayesian theorem [21] provides a mathematical framework. Event B is defined as the attainment of the target frequency, and event H is defined as the occurrence when the coherence value is greater than or equal to a certain value (i.e., the threshold). The likelihood $P(H|B)$, represents the probability that, when the target frequency is known, its corresponding coherence value is greater than the threshold. The prior $P(B)$, is the probability of attaining the target frequency in the absence of a threshold, whereas the evidence $P(H)$, is the probability that the coherence value is greater than the threshold. The posterior $P(B|H)$, that is, the probability that the target frequency can be obtained when the threshold is given, can be calculated as:

$$P(B|H) = \frac{P(H|B)\hat{A}\cdot P(B)}{P(H)} \tag{3}$$

The 0–50 Hz frequency range is uniformly divided into q intervals (θ_1, θ_2…,θ_q), each corresponding to a $\frac{50}{q}$ interval. Subsequently, a frequency interval $\theta \in [F_i, F_j]$ can be defined, within which the bridge frequency is contained; the event B_θ can be denoted as the identification of the bridge frequency. Assuming that the coherence matrix $[X]$ contains a sufficient amount of data and letting t be the percentile where the threshold resides, event $H(t)$ represents the occurrence when the coherence value is greater than t, with the corresponding probability being $P[H(t)]$. $P[H(t)|B_\theta]$ represents the probability that, when the bridge frequency is known, its corresponding coherence value is greater than t. The probabilities $P[H(t)|B_\theta]$ and $P[H(t)]$ belong to the probability density distributions $D_1(t)$ and $D_2(t)$, respectively, and $P(B_\theta)$ equals a constant value φ. For two discrete distributions, the original Bayesian equation can be expressed as:

$$P[H(t)|B_\theta] = \int_t^1 D_1(t)dt \approx \sum_{k=0}^{w-1} D_1\left(t + \frac{1-t}{w}k\right)\frac{1-t}{w} \tag{4}$$

$$P[H(t)] = \int_t^1 D_2(t)dt \approx \sum_{k=0}^{w-1} D_2\left(t + \frac{1-t}{w}k\right)\frac{1-t}{w} \tag{5}$$

$$M(t) = P[(B_\theta|H(t))] = \frac{P[H(t)|B_\theta]\cdot\varphi}{P[H(t)]} = \frac{\varphi\sum_{k=0}^{w-1} D_1\left(t+\frac{1-t}{w}k\right)\frac{1-t}{w}}{\sum_{k=0}^{w-1} D_2\left(t+\frac{1-t}{w}k\right)\frac{1-t}{w}} \tag{6}$$

In these equations, w represents the number of divisions in the discrete distribution. For example, with an interval of 0.01 (1%), the value of w is 100.

Now, the problem of threshold selection is transformed into finding a value that maximizes the target function. Let τ be the value that maximizes the target function $M(t)$, such that:

$$\tau = \text{argmax}_t M(\tau) \tag{7}$$

When the distributions $D_1(t)$ and $D_2(t)$ are known, iterative algorithms can be employed to determine this τ. The algorithm designed in this study is illustrated in Fig. 2, where the initial threshold t, is set to 0,

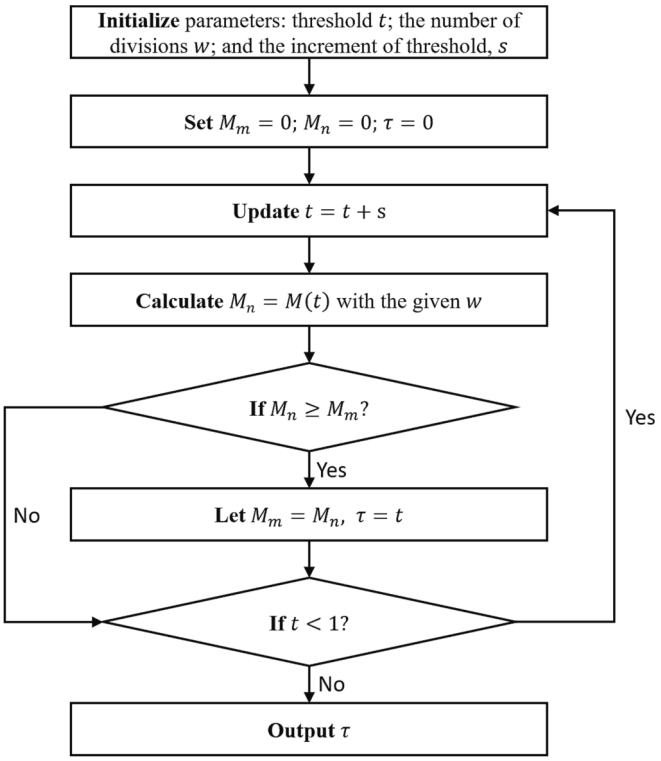

Fig. 2. Iterative algorithm.

number of divisions w, is 100, and threshold increment s, is 0.01. This is the strategy used in this study to find the threshold. Although a mathematical framework for this method is provided herein, in practical cases, obtaining $D_1(t)$ can sometimes be challenging. In such cases, empirical thresholds can be adopted as discussed in the following sections.

2.3. Step 3: Selection of PPs and frequency identification

This step counts the probability of each frequency interval above the threshold. Dividing the 0–50 Hz frequency range into 100 intervals (θ_1, $\theta_2 \ldots, \theta_{100}$), each corresponding to a 0.5 Hz interval, ideally the interval, θ, containing the bridge frequency will exhibit the maximum probability value, $M(\tau)$.

During the operation, the peaks in the coherences above the threshold P_i, and their corresponding frequencies F_i, are collected to construct a new matrix $[P]$ (e.g., a prominent peak matrix):

$$\begin{bmatrix} P_1 P_2 \cdots P_n \\ F_1 F_2 \cdots F_n \end{bmatrix} = [P] \tag{8}$$

Then, the PP occurrence in each frequency interval is counted. The interval corresponding to the maximum occurrence indicates the fundamental frequency of the bridge. This process entails finding the peaks in the PP distribution (see Fig. 3); in this step, the bridge frequency is deemed identifiable.

Notably, this methodological framework is premised on the availability of large amounts of data, and the identified frequency is a statistical result. That is, when selecting the threshold, the amount of data retained after threshold truncation must be statistically sufficient to demonstrate the result. This is discussed in the following sections.

3. Numerical study

To verify the proposed bridge frequency identification algorithm and investigate the influences of various factors, numerical studies, including VBI simulations and the Monte Carlo method [22], were carried out. The following describes the formulation of the VBI system, simulation of road roughness, and addition of environmental noise. The factors considered in method validation included road roughness, environmental noise, vehicle parameter variation, and number of runs. The goal was to investigate the effectiveness and robustness of the proposed algorithm under various factors.

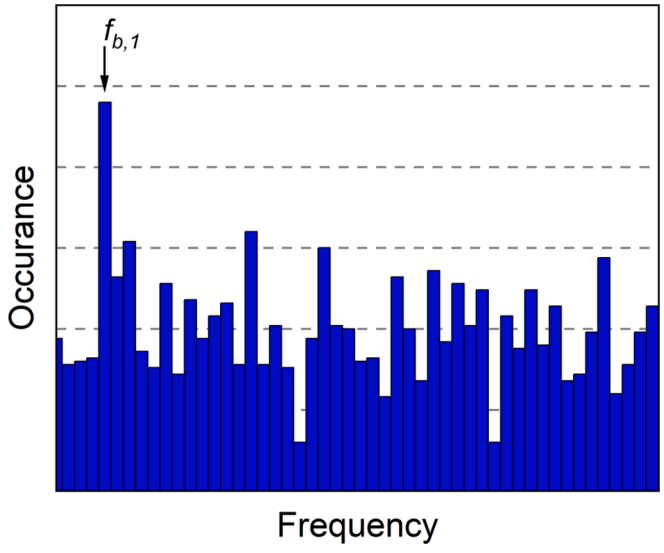

Fig. 3. PP distribution.

3.1. VBI formulation

Several models have been developed to simulate the VBI process. Some authors have modelled the vehicle as a single vertical force or as a series of constant forces [23], whereas others have considered the vehicle as a lumped sprung mass model [5,24]. A more comprehensive vehicle model is the 2 degrees of freedom (DOF) quarter-car model, in addition to the 4-DOF models [6,25,26]. In this study, a 2-DOF quarter-car model was employed to represent the rear axle system of the bus (see Fig. 4). This simplification was used in the study by Liu et al. [13], who showed that neglecting the excitation of the front suspension vibration at the rear axle system is equivalent to adding a certain amount of noise to their results, which is acceptable. An unconventionally high level of noise (noise level = 10%) was adopted in this study, whereas previous research often considered 5% as a high noise level [27,28]. The utilization of this model is advantageous in that it enables a good trade-off between model complexity and computational efficiency, which facilitates the implementation of computationally demanding methods such as Monte Carlo simulations.

The bridge model used in this study was a simply supported Euler–Bernoulli (EB) beam. Each node of its finite element (FE) model consisted of two DOFs: vertical translation and rotation. The bridge model is composed of n elements, $n+1$ nodes, and $2n$ DOFs (excluding the vertical constraints at either end). It has a length of L, uniform flexural rigidity of EI, and mass per unit length of m. Additionally, the damping of the bridge is approximated by mass-stiffness proportional Rayleigh damping. The VBI model used in this study is shown in Fig. 5. The governing coupled equations for the VBI system are given by:

$$[M_v]\left\{\ddot{y}_v\right\} + [C_v]\left\{\dot{y}_v\right\} + [K_v]\{y_v\} = \{F_{cv}\} \tag{9}$$

$$[M_b]\left\{\ddot{y}_b\right\} + [C_b]\left\{\dot{y}_b\right\} + [K_b]\{y_b\} = \{F_{cb}\} \tag{10}$$

where (9) and (10) are the equations of motion associated with the vehicle and the bridge, respectively. Matrices $[M_v]$, $[C_v]$ and $[K_v]$ correspond to the mass, damping, and stiffness of the vehicle, respectively, whereas $[M_b]$, $[C_b]$ and $[K_b]$ represent the mass, damping, and stiffness matrices of the bridge model, respectively. In these equations, $\{y_v\}$ denotes the displacement vector of the vehicle, and $\{y_b\}$ is the nodal displacement of the bridge system. Additionally, $\{F_{cv}\}$ and $\{F_{cb}\}$ represent the time-varying interaction forces on the vehicle and bridge, respectively.

The subsystem matrices and response vector for the vehicle model are as follows, where the body and axle masses are denoted by m_v and m_t, the suspension and tire damping by c_s and c_t, and the suspension and tire stiffness by k_s and k_t, respectively. The vertical displacements of the vehicle body and axle are denoted u_v and u_t, respectively.

$$[M_v] = \begin{bmatrix} m_v & \\ & m_t \end{bmatrix} \tag{11}$$

$$[C_v] = \begin{bmatrix} c_s & -c_s \\ -c_s & c_s + c_t \end{bmatrix} \tag{12}$$

$$[K_v] = \begin{bmatrix} k_s & -k_s \\ -k_s & k_s + k_t \end{bmatrix} \tag{13}$$

$$\{y_v\} = \begin{bmatrix} u_v & u_t \end{bmatrix}^T \tag{14}$$

The Newmark-Beta method was used to obtain the dynamic responses of the vehicle through the VBI process. The parameters β and γ of the Newmark-Beta method are selected as 0.25 and 0.5, respectively, as suggested by many studies [1,27,29].

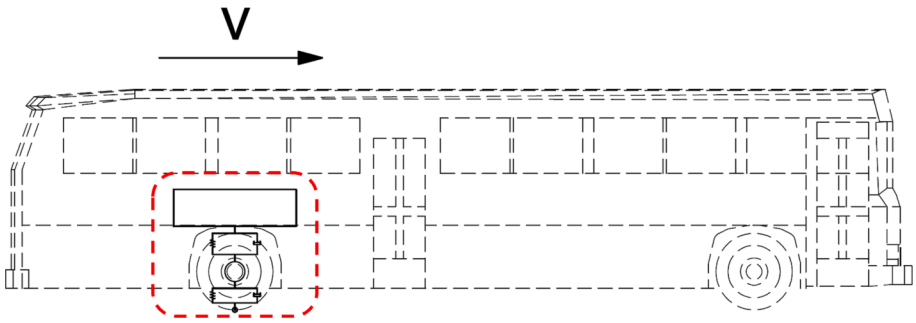

Fig. 4. Simplified model for rear axle system.

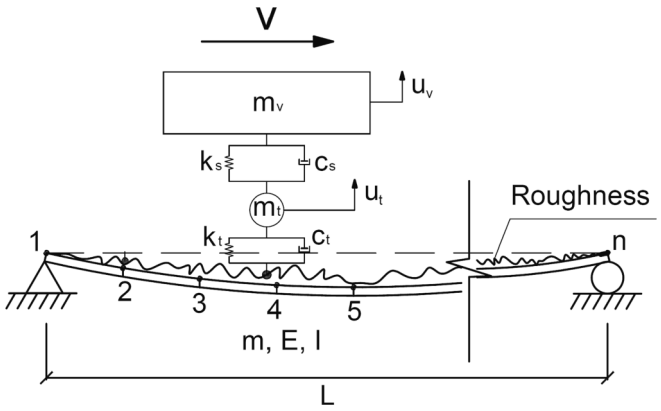

Fig. 5. VBI model.

3.2. Simulation of road roughness

In this study, road roughness was simulated according to ISO 8608 [30], which can be characterized using a power spectral density (PSD) function given by [27]:

$$G_d(n_s) = G_d(n_{s,0})\left(\frac{n_s}{n_{s,0}}\right)^{-\omega} \tag{15}$$

where n_s represents the spatial frequency and $n_{s,0}$ is the reference spatial frequency set at 0.1 m^{-1}. The constant ω equals 2, and the roughness coefficient $G_d(n_{s,0})$, is determined based on different roughness classes [31]. Table 1 presents the five roughness classes that could potentially arise in engineering applications, along with their corresponding roughness coefficients.

A standard zero-mean real-valued stationary Gaussian process can then be used to simulate the surface roughness profile as follows:

$$r(x) = \sum_{i=0}^{N} \sqrt{2G_d(n_{s,i})\Delta n_s}\cos(2\pi n_{s,i}x + \varphi_i) \tag{16}$$

where N denotes the number of harmonic waves used to construct the roughness profile. $n_{s,i}$ represents the i-th spatial frequency, while $\Delta n_s = 0.01\text{cycle/m}$ is the sampling interval of the spatial frequency. φ_i represents the random phase angle of the i-th cosine function, which is sampled uniformly at random from the interval $[0, 2\pi]$.

Table 1
Roughness coefficient for different roughness classes.

Class	A	B	C	D	E
$G_d(n_{s,0})/10^{-6}m^3$	$0-2^5$	2^5-2^7	2^7-2^9	2^9-2^{11}	$2^{11}-2^{13}$

3.3. Addition of environmental noise

Another primary source of noise, environmental noise, can be added to the vehicle acceleration signal in the form of Eq. (17) [27,32]. where $\ddot{u}_p$ represents the polluted acceleration data, E_p is the noise level, N_s is the standard normal distribution, and $\sigma_{\ddot{u}_v}$ is the standard deviation of the vehicle response $\ddot{u}_v$.

$$\ddot{u}_p = \ddot{u}_v + E_p N_s \sigma_{\ddot{u}_v} \tag{17}$$

3.4. Numerical results: Pure VBI process

Simulations were conducted to validate the proposed algorithm using the VBI model described above. The initial vehicular parameters were adopted from Nagayama et al. [1] with some modifications to represent a truck or bus. The specific parameters are: $m_v = 1.0 \times 10^4$ kg, $m_t = 1.0 \times 10^3$ kg, $c_s = 1.0 \times 10^4$ N s/m, $c_t = 0$, $k_s = 4.0 \times 10^5$ N/m, $k_t = 3.5 \times 10^6$ N/m, and $v = 7.5$ m/s. Further discussion on the impact of variations in vehicular parameters on the results is presented in the following sections. The bridge parameters are: $m = 2000$ kg/m, $EI = 6.06 \times 10^{10}$ N m^2, $L = 45$ m. Additionally, the sampling rate in the simulation is 1000 Hz (or the time step is 0.001 s). It should be noted that the purpose of this section is only to verify the method and not to reproduce the actual behavior of the field test.

First, a pure VBI process without road roughness or environmental noise was studied. The VBI model presented herein simulates the rear axle system of a bus. The vehicle response used in the simulation was $\ddot{u}_t$, which corresponds to the accelerations captured by the sensor mounted on the rear axle in the on-site experiments. As shown in Fig. 6a, under ideal conditions, the vibration response of the rear axle tends to "mimic" bridge vibration to some extent. This is more apparent in the frequency spectrum (see Fig. 6b), where the first and second mode frequencies of the bridge are clearly identifiable in the vehicle's frequency spectrum, although the amplitude in the vehicle is lower. In this scenario, the 1st modal frequency of the bridge can be identified as the largest peak in the vehicle spectrum, which is used as a reference value for the following scenarios. Notably, the vehicle frequency appeared to be indistinguishable from the spectrum in this case. This is primarily because of the high damping adopted in the vehicle model. In fact, commercial vehicles, such as buses, often have high damping, and obtaining their frequencies usually involves errors or is even impossible. The high damping value used in this study aligns with engineering practice.

3.5. Numerical results: Common VBI scenarios

In practice, vibrational components from sources of road roughness and environmental noise usually dominate the vehicle responses. Employing the vehicle and bridge parameters above, and considering "A" class road roughness and 10% environmental noise, the responses of the vehicle and bridge are shown in Fig. 7. Although some peaks appeared to be related to the bridge frequency, it was difficult to determine the bridge frequency from the frequency spectrum.

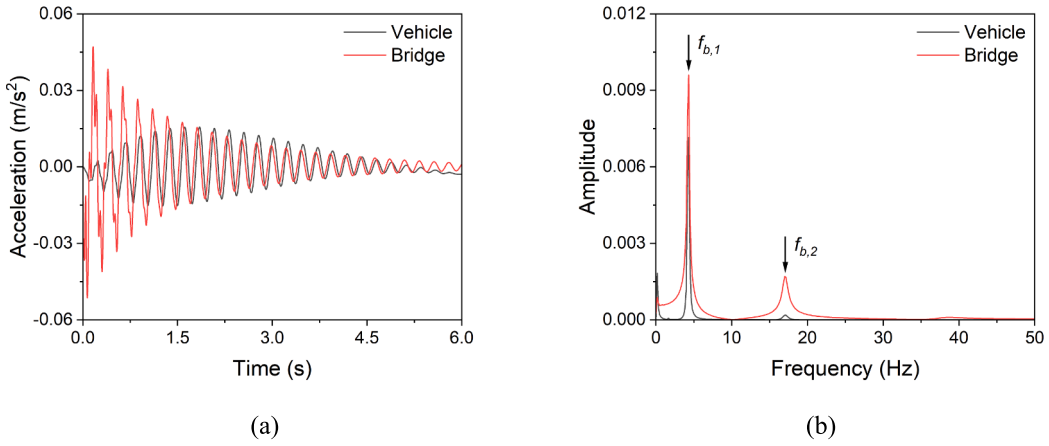

Fig. 6. Pure VBI responses: (a) time-domain response, (b) frequency-domain response.

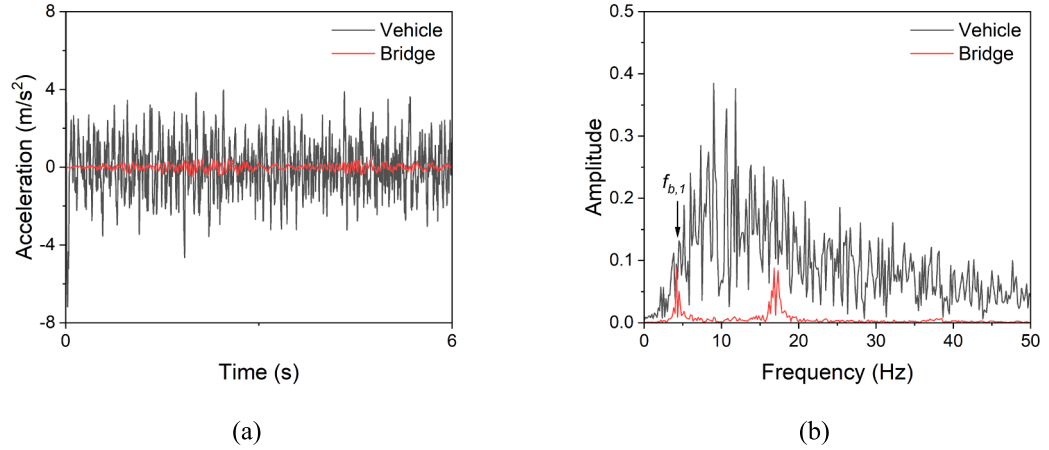

Fig. 7. VBI responses in common scenarios: (a) time-domain response, (b) frequency-domain response.

The application of the proposed algorithm can be demonstrated by assuming that the bridge frequency is the most common vibrational component across different vehicle passes. When applying the proposed algorithm, in addition to considering road roughness and environmental noise, variations related to the speed and weight of the vehicle (e.g., potentially varying passenger loads for a bus) should be considered. These are expressed in the following forms:

$$m_{v,i} = m_{v,0} + N_u m_d \tag{18}$$

$$v_i = v_0 \pm N_u v_d / 2 \tag{19}$$

where $m_{v,i}$ and v_i are the body mass and speed of the vehicle in the i-th

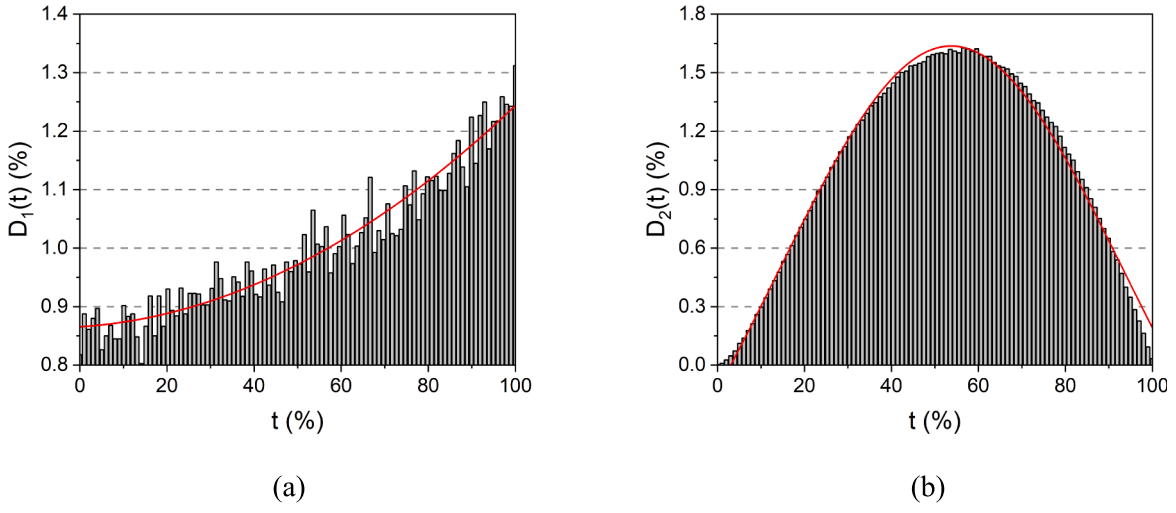

Fig. 8. Density distributions: (a) $D_1(t)$, (b) $D_2(t)$.

run, $m_{v,0}$ and v_0 represent the initial body mass and speed of the vehicle, respectively. m_d and v_d are the deviations in the weight and speed for all vehicle runs, respectively, and N_u represents a uniform distribution in the interval [0,1]. It is thought that a conventional bus can carry up to 80 passengers [33]. Considering that the average weight of passengers is 70 kg and the rear axle bears half of the weight, the weight deviation, m_d, can be taken as 2800 kg. The speed of buses varies across regions and periods. According to our field measurements, the approximate speed deviation for passing through the same bridge was 5 m/s.

The probability density distribution of $P[H(t)|B_\theta]$, denoted as $D_1(t)$, can be obtained (zero values in the coherences are not counted and are the same below) by running 100 simulations of vehicle passages on the roughest road profile (E class), as shown in Fig. 8a. Even in the roughest case, bridge frequency was more likely to be in the higher percentiles, which is consistent with this assumption. The probability density distribution of $P[H(t)]$, $D_2(t)$, appeared normal, as shown in Fig. 8b. The algorithm presented in Fig. 2 can be used to compute $P[(B_\theta|H(t))]$ and find τ (see Fig. 9). This indicates that the maximum value of $P[(B_\theta|H(t))]$ should be obtained at a large t value. For larger values of t, the result increases as t increases; however, sufficient data must be retained to ensure the statistical significance of the final results.

According to the 3-Sigma rule in statistics [34], that is, in a normal distribution, approximately 68% of the observations fall within one standard deviation from the mean ($\tau = 0.84$), 95% fall within two ($\tau = 0.975$), and 99.7% fall within three ($\tau = 0.9985$). By simply estimating that we need 100 data points above the threshold to ensure the significance of the results, the above three τ values require 48, 264, and 781 vehicle passages, respectively. Collecting hundreds of passages may take weeks for a city bus to operate normally, during which time factors, such as temperature, could change the bridge frequency. Thus, $\tau = 0.84$ may be chosen as the threshold in this study, striking a tradeoff between ensuring $P[(B_\theta|H(t))]$ and retaining the amount of data.

The probability distributions across all roughness cases are found to be similar, with $D_1(t)$ having bridge frequency likely in the higher percentiles, and $D_2(t)$ is roughly normal. The distribution of $D_1(t)$ appears to be unaffected by the road roughness. The near-normal distribution of $D_2(t)$ may be associated with the road roughness simulation based on the Gaussian process as well as the noise simulation generated from the Gaussian distribution. Nevertheless, the mathematical framework of the method does not depend on a particular distribution. In practice, a relatively large threshold can be selected empirically, as long as the assumption that the bridge frequency is more likely to be in the higher percentiles holds true.

As seen in Fig. 10, the largest peak in the PP distribution obtained by the proposed algorithm can clearly indicate the bridge frequency across all levels of road roughness, i.e., $\theta \in [3.5\,Hz, 4.5\,Hz]$. The frequency of the bridge was 4.2 Hz. Owing to many factors (e.g., vehicle weight), under the normal operation of a bridge, its frequency may fluctuate within a small range. This is a common problem with the drive-by approach; the bridge frequency extracted from the car is not necessarily the same as the bridge frequency in free vibration. For example, considering only the situation where the vehicle has the greatest influence on the bridge frequency (when the vehicle is at the midpoint of the span), the 1st mode frequency of a simply-supported-beam bridge can be theoretically estimated using Eq. (20) [35]. In this equation, ω_v and ω_b can be computed as $\omega_v = f_{v,1} \times 2\pi$ and $\omega_b = f_{b,1} \times 2\pi$ respectively, representing the original frequencies of the vehicle and bridge. Other variables present the same as previously defined.

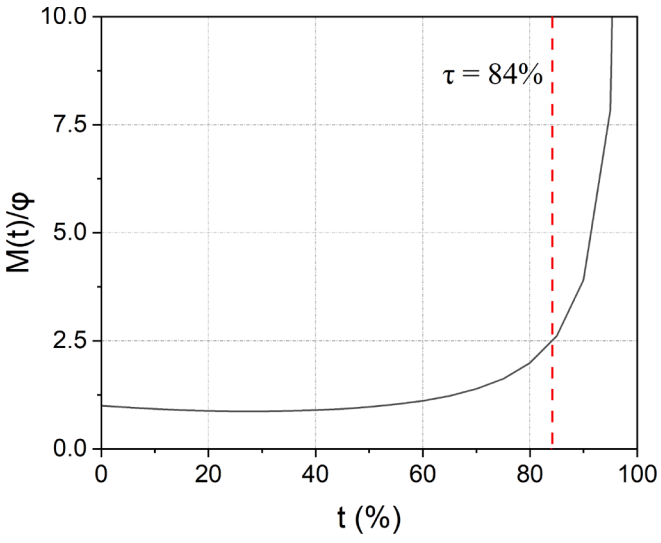

Fig. 9. Computed results from Iterative algorithm.

$$\breve{\omega}_b^2 = \frac{\omega_v^2}{2} + \frac{\omega_b^2}{2} + \frac{M_v\omega_v^2}{mL} + \sqrt{\left(\frac{\omega_v^2}{2} + \frac{\omega_b^2}{2} + \frac{M_v\omega_v^2}{mL}\right)^2 - \omega_v^2\omega_b^2} \tag{20}$$

Through calculations, factoring in the maximum and minimum vehicle weights, the bridge frequency range would lie between 4.22 and 4.24 Hz, which falls within the identified range.

3.6. Numerical results: Effect of driving cycles

The effect of the number of vehicle passes on the results is also investigated. Utilizing the same vehicle and bridge parameters as before, 10% environmental noise, and the variations in vehicle speed and weight, the algorithm results are depicted in Fig. 11, while considering "E" class road roughness. When the results are obtained from a smaller number of vehicle passes, the peaks associated with the bridge frequency may not be identified well. Hence, the driving cycles should ensure statistical significance of the results.

The prominence index, *PI*, coefficient of variation, *CV*, and clarity index, *CI*, can be defined using Eqs. (21), (22), and (23), to evaluate the results of the PP distribution obtained using the algorithm. Generally, a higher *PI* value indicates a more prominent maximum peak (the maximum peak value is much higher than all the other values), and a lower *CV* value indicates a more stable distribution. The clarity index, *CI*, composed of both measures, can be used to some extent to assess the reliability of results, with higher values indicating more reliable outcomes.

$$PI = P_{max}/\mu_p \tag{21}$$

$$CV = \sigma_p/\mu_p \tag{22}$$

$$CI = PI/CV \tag{23}$$

where P_{max} is the largest peak value of the PP distribution, μ_p is the mean value of the PP distribution, and σ_p represents the standard deviation of the PP distribution.

Table 2 lists the indices corresponding to the numbers of selected vehicles. When the number of runs was relatively small (e.g., 10 runs), the maximum peak did not point to the bridge frequency, and the noise peak dominated the distribution. In this case, the *PI* is directed towards the noise peak, which was relatively high (1.50), and the *CV* value was the highest (0.26), leading to a low *CI* value (5.77). As the number of runs increased, the maximum peak shifted towards the bridge frequency. The *PI* value stabilizes between 1.33 and 1.41, while the *CV* value gradually decreases and then stabilizes (0.12–0.13). Meanwhile, the *CI* value increases and tends to stabilize (10.62–11.08), representing reliable results after about 50 runs.

3.7. Numerical results: Monte Carlo simulation

Considering the fact that bridge monitoring is a long-term process, and that vehicles, especially buses, may experience parameter variations

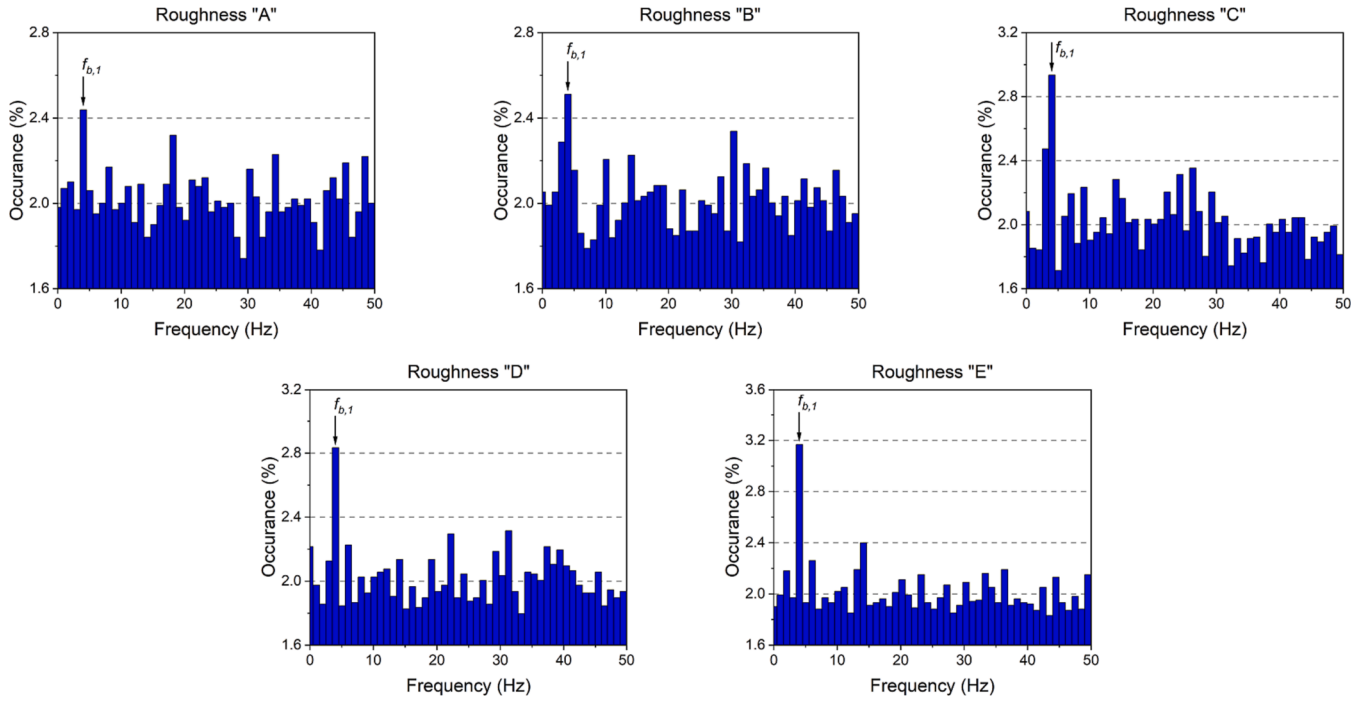

Fig. 10. Distribution of PPs for different roughness classes obtained from the proposed algorithm.

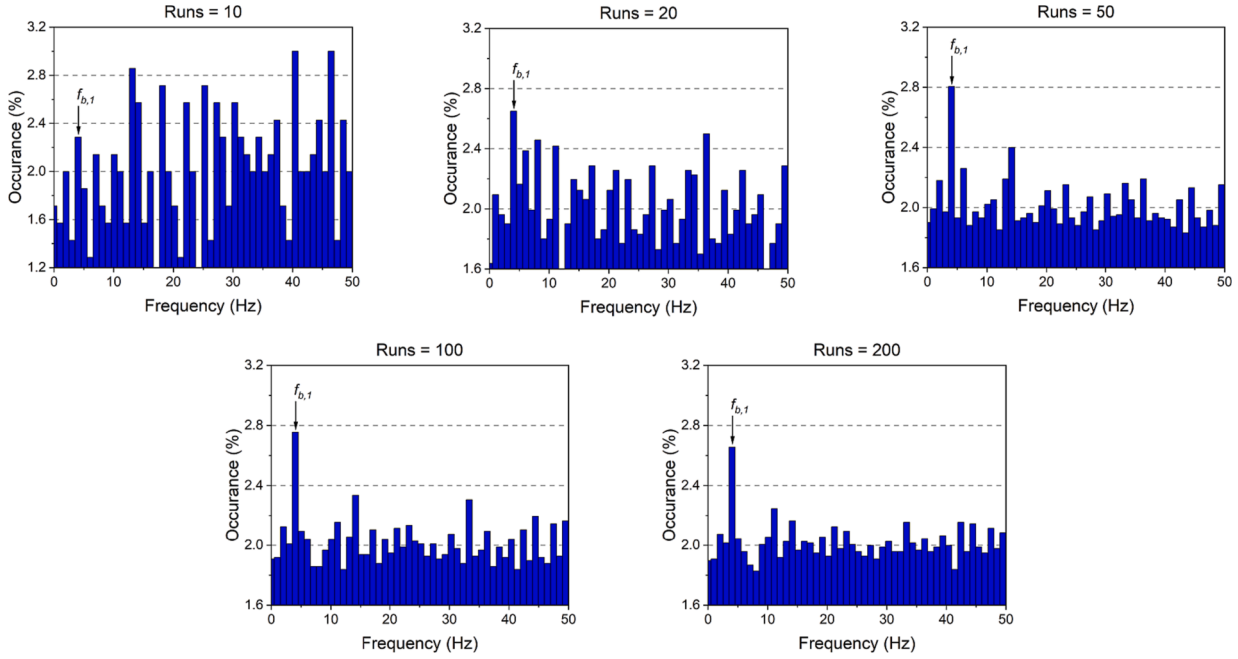

Fig. 11. Distribution of PPs for different vehicle runs.

Table 2
Indexes corresponding to the number of runs.

Runs	10	20	50	100	200
PI	1.50	1.33	1.41	1.38	1.33
CV	0.26	0.16	0.13	0.13	0.12
CI	5.77	8.31	10.85	10.62	11.08

other than speed and weight during long-term operation, this section uses a Monte Carlo simulation to validate the effectiveness of the proposed algorithm under complex parameter variations. The underlying concept of the Monte Carlo simulation is to use randomness to solve problems that might be deterministic in principle [22]. Vehicle parameters that need to be considered based on the above model, in addition to speed and weight, include axle mass, suspension, and tire damping, as well as suspension and tire stiffness. These are expressed as follows:

$$m_{t,i} = m_{t,0} \pm N_u dm_{t,0} \tag{24}$$

$$c_{s,i} = c_{s,0} \pm N_u dc_{s,0} \tag{25}$$

$$c_{t,i} = c_{t,0} \pm N_u dc_{t,0} \tag{26}$$

$$k_{s,i} = k_{s,0} \pm N_u d k_{s,0} \tag{27}$$

$$k_{t,i} = k_{t,0} \pm N_u d k_{t,0} \tag{28}$$

where $m_{t,i}$, $c_{s,i}$, $c_{t,i}$, $k_{s,i}$, and $k_{t,i}$ are the axle mass, suspension damping, tire damping, suspension stiffness, and tire stiffness at the i-th run, respectively, whereas $m_{t,0}$, $c_{s,0}$, $c_{t,0}$, $k_{s,0}$, and $k_{t,0}$ denote the initial parameters of them. N_u represents a uniform distribution in the interval [0,1], and d stands for the maximum degree of deviation that may occur during long-term operation.

Here, using the initial vehicle parameters and environmental noise conditions (10% noise level), as described earlier, we considered the possibility of a 25% variation ($d = 0.25$) in each vehicle parameter during long-term operation. Based on the results presented in Table 2, 50 or more runs are sufficient to obtain a good algorithm performance. Random parameters are used to generate samples via the VBI simulations, with 50 samples (i.e., 50 vehicle passes) as one algorithm input, denoted by $[X]_q$ (q = 1, 2, 3…), and the output is $P_q(B_\theta|H_\tau)$. When the algorithm is run 2000 times for each road roughness, the Monte Carlo result for that roughness level should be $\frac{1}{2000}\sum_{q=1}^{2000} P_q(B_\theta|H_\tau)$, and the likelihood would be $\frac{1}{2000}\sum_{q=1}^{2000} P_q(H_\tau|B_\theta)$, that is, the cumulative probability of $D_1(t)$ (see Fig. 12a). As shown in Fig. 12b, the evidence is that $\frac{1}{2000}\sum_{q=1}^{2000} P_q(H_\tau)$, which is the cumulative probability of $D_2(t)$. As shown in Fig. 12a, the bridge frequency was more likely to be in the higher percentiles across all roughness levels under complex scenarios involving the changes in all vehicle parameters and the presence of environmental noise, and their distributions exhibited substantial similarity. Fig. 12b clearly shows the near-normal distribution of the coherence values across various cases. Accordingly, the PP distributions were similar, even under complex scenarios involving the changes in all the vehicle parameters and the presence of environmental noise (see Fig. 13).

As shown in Table 3, upon the introduction of a variety of variable parameters, the *CI* values in the Monte Carlo results were high, affirming their reliability. Thus, the effectiveness of the algorithm under general conditions was validated using the Monte Carlo method. Furthermore, in contrast to the previous studies that aimed to avoid differences (e.g., by trying to reduce variation, driving in the same lane, and using the same speed), these findings encourage the deliberate addition of variability to filter bridge frequencies, making this approach particularly attractive in practical engineering applications. Another insight is that measurements obtained from multiple distinct vehicles can filter the bridge-related components in the signal, because the distinct characteristics of each vehicle infuse variability into the non-bridge components of the signals. There is an existing body of research focused on crowd-sensing vehicle monitoring; however, most of these studies are currently in the theoretical or laboratory experimental stages [36,37]. This study corroborates their feasibility from a unique perspective.

4. Field test verification

4.1. Description

In 2018, field experiments were conducted on two bridges located in Finland, namely the Olari and Matti bridges, as shown in Figs. 14 and 15. The Olari Bridge is a three-span continuous bridge, with some of its parameters listed in Table 4. The Matti Bridge is a four-span continuous bridge, and a few of its parameters are listed in Table 5. Sensors were placed on the bridge structure for direct measurements to obtain the actual frequencies of the bridge as a reference. The accelerometers used were PCB model M352C68, the data acquisition device used was NI9234, and the measurement software employed was PC + LabVIEW. The sampling frequency for the measurements was set to 1650 Hz.

For the measurement vehicles, buses from the Finnish company HSL, serving the urban public transportation system, were used, as illustrated in Fig. 16a. The empty vehicle weight was approximately 1.51×10^4 kg, and the sensors were installed on the rear axle of the bus (see Fig. 16b). The accelerometers used on the bus were the same as those on the bridge, namely PCB's model M352C68. The data acquisition system was the imc Cronos PL2, and the measurement software was the PC + imc STUDIO. The sampling frequency for the measurements was set at 1000 Hz. The sensors continuously collected data during the bus's operation, and instances of crossing the bridges were subsequently selected from the measured data. The measurements were performed by repeatedly driving the bus along the same route in the same direction. Olari bridge was crossed 12 times, and Matti bridge was crossed 13 times.

When employing the proposed algorithm, the signal segments should be of equal length (i.e., the same time period) to ensure that they have the same frequency resolution. In this study, equal-length signal segments were used across various bus passes (3 s segment). Notably, these segments should be selected from the signal sections where the entire

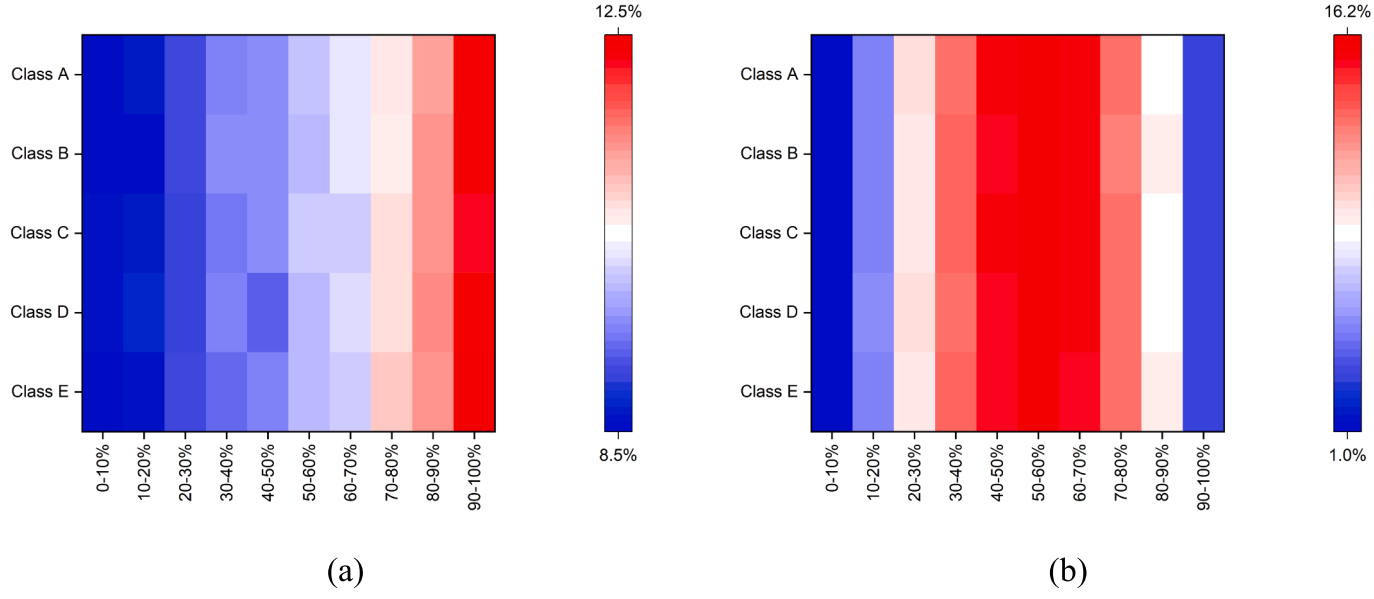

Fig. 12. Cumulative probabilities of: (a) $D_1(t)$, (b) $D_2(t)$.

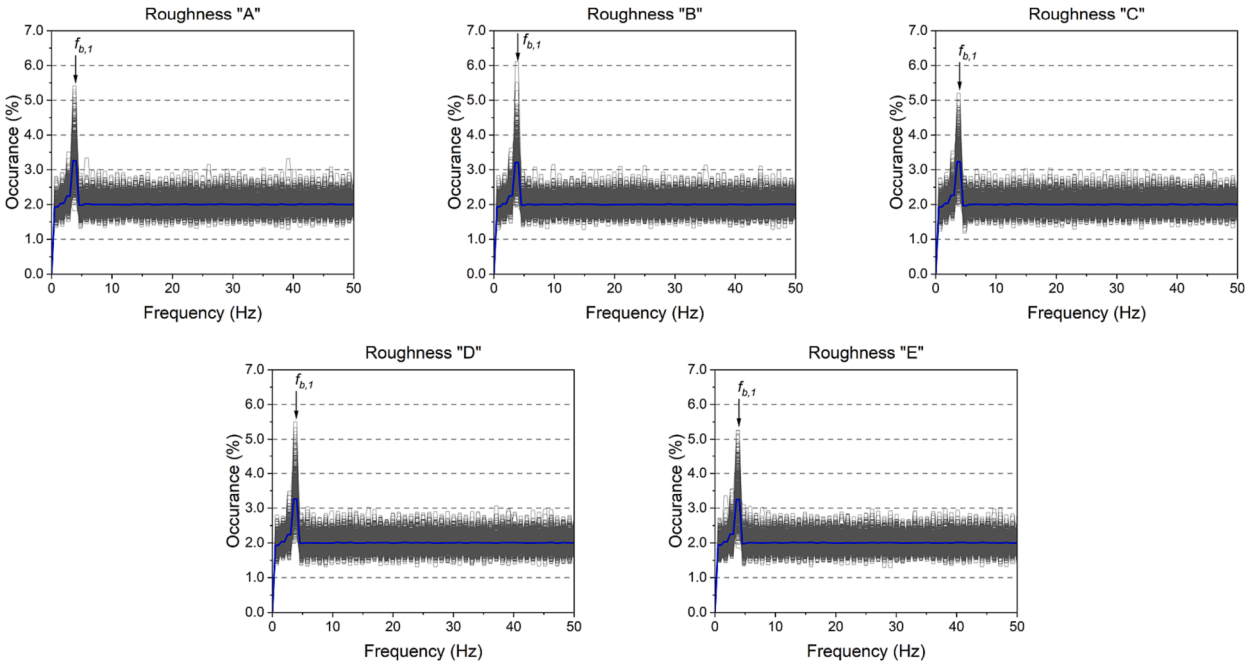

Fig. 13. Distribution of PPs for different vehicle runs obtained by Monte Carlo methods.

Table 3
Mean indexes corresponding to roughness classes.

Roughness class	A	B	C	D	E
PI	1.62	1.60	1.61	1.62	1.62
CV	0.13	0.13	0.13	0.13	0.13
CI	12.01	12.02	12.00	12.01	12.01

bus is on the bridge. Two criteria are used to identify the signal segment where the bus is on the bridge. First, as shown in Fig. 17, the position of the bus can be mapped well using GPS data. Using this information, we can approximately segment the period when the bus is on the bridge. Second, as depicted in Fig. 18, when the bus passes over the expansion joints of the bridges, noticeable peaks in the acceleration signals can be observed, which can also be used as an indicator. By correlating these, the desired signal segment can be cut off.

4.2. Field test results

Fig. 19 presents examples of the spectra obtained from the Fast Fourier Transform (FFT) processing of the accelerometers on both the bridge and vehicle, with similar results observed in other samples. Although there appear to be peaks associated with bridge frequencies in the vehicle's spectrum, it is relatively challenging to directly extract the bridge frequencies from it. Another important piece of information is that the frequencies of the Olari and Matti bridges can be obtained from the spectra of the direct bridge measurements at approximately 10.2 Hz and 10.6 Hz, respectively. These frequencies were used as references to evaluate the results of the algorithm.

Considering their complete traversals of 12 and 13 times, the computed outcomes for the Olari and Matti bridges utilizing the algorithm are shown in Fig. 20. The bridge frequency peaks stand out within the distribution of PPs, and their values correspond to the outcomes of the direct measurements. As shown in Table 6, the *CI* values for the Olari and Matti bridge are 7.29 and 8.19, respectively, which are close to the scenario involving 20 runs in the simulation results. This suggests that

Fig. 14. Olari bridge: (a) side view, (b) pavement surface on bridge deck.

(a) (b)

Fig. 15. Matti bridge: (a) side view, (b) pavement surface on bridge deck.

Table 4
Olari bridge.

Parameter	Details
Number of spans	3
Lengths of spans	17.5 m + 27 m + 17.5 m
Length of deck	65 m
Min useful width	26.12 m

Table 5
Matti bridge.

Parameter	Details
Number of spans	4
Lengths of spans	11 m + 21 m + 19.99 m + 16 m
Length of deck	69 m
Min useful width	38.05 m

the proposed algorithm provides satisfactory performance and applicability in the real-world implementation of buses for examining bridges. It is noteworthy that in addition to augmenting the number of vehicle traversals to enhance the identification performance, additional prior information, such as a rough range for bridge frequencies, could also contribute to bridge frequency identification in real-world scenarios. Overall, the findings of this field experiment validated the robustness and practicality of the proposed algorithm.

5. Conclusion

This paper proposes a coherence-PPI algorithm based on the Bayesian framework and applies it to city bus monitoring for bridge frequency identification. The algorithm consists of three steps. First, the coherences were calculated for all vehicle runs to interpret the signal relations. Second, a Bayesian framework was established to statistically determine the threshold. Third, the PPs were selected based on the threshold and their distribution was counted to identify the bridge frequency. The underlying idea is to recognize the bridge frequency as a common vibration component across various vehicle runs. The

(a) (b)

Fig. 16. City bus for field tests: (a) the view of the bus, (b) sensor installation.

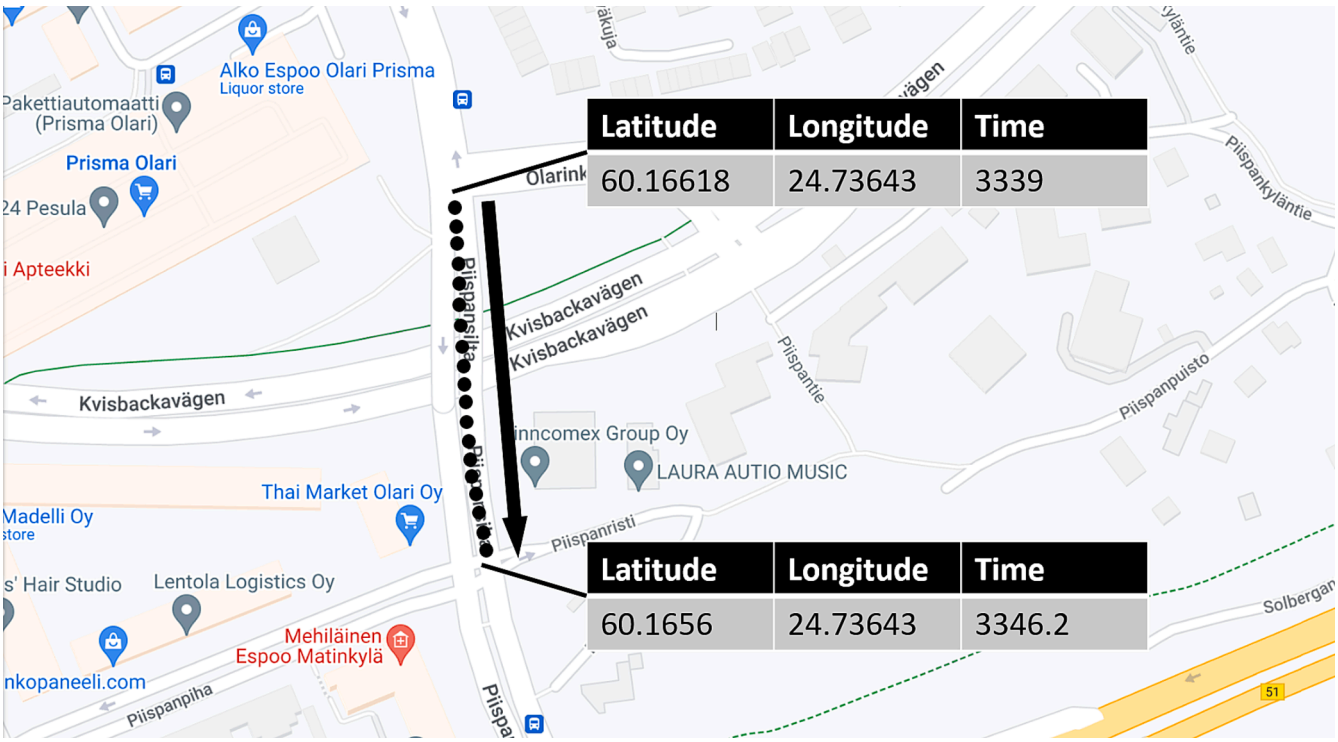

Fig. 17. GPS mapping.

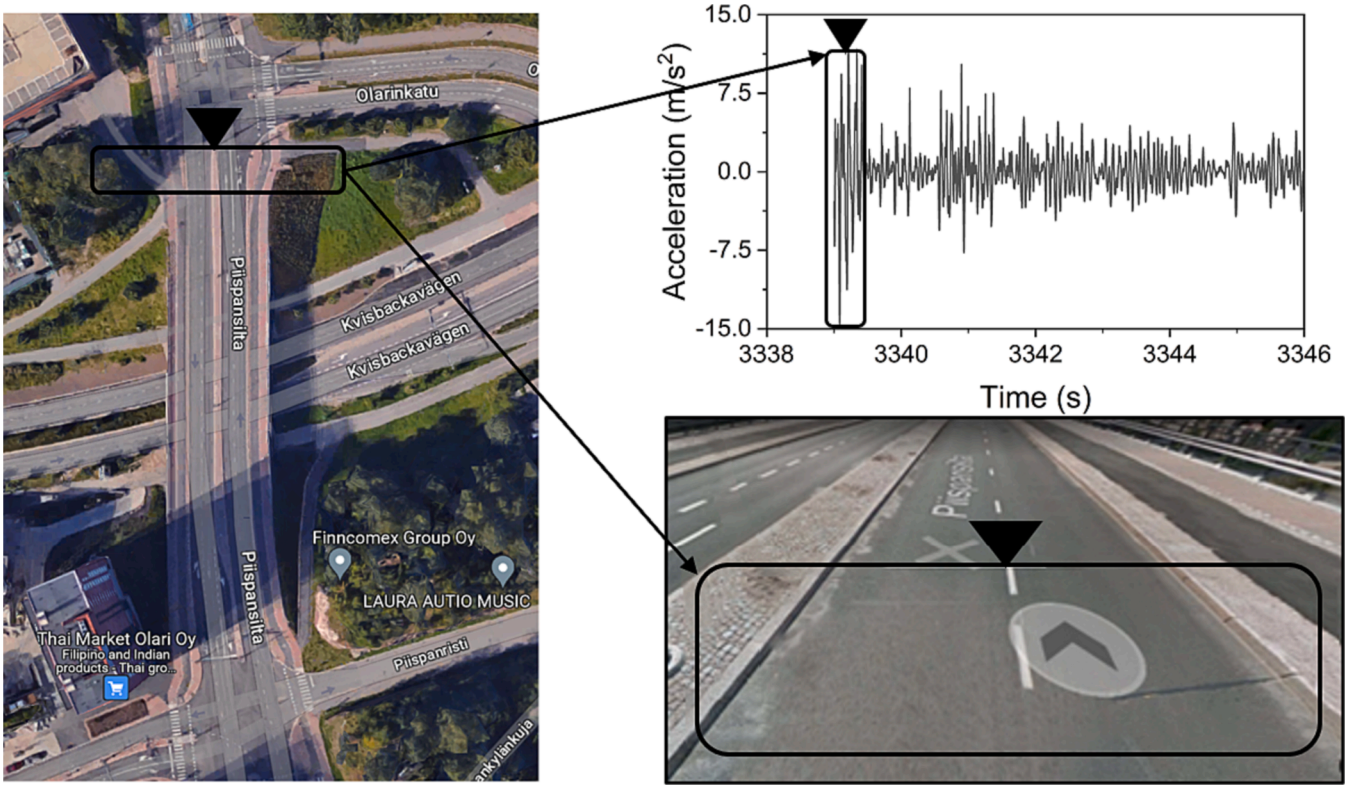

Fig. 18. Selection of bus acceleration signals.

effectiveness and robustness of the proposed algorithm were investigated through numerical simulations and field tests employing a city bus, leading to the following conclusions:

(1) Under the influence of road roughness and environmental noise, the fundamental frequency of the bridge can be successfully identified as the largest peak in the algorithm results based on bus responses, which is consistent with the results obtained through direct measurements.

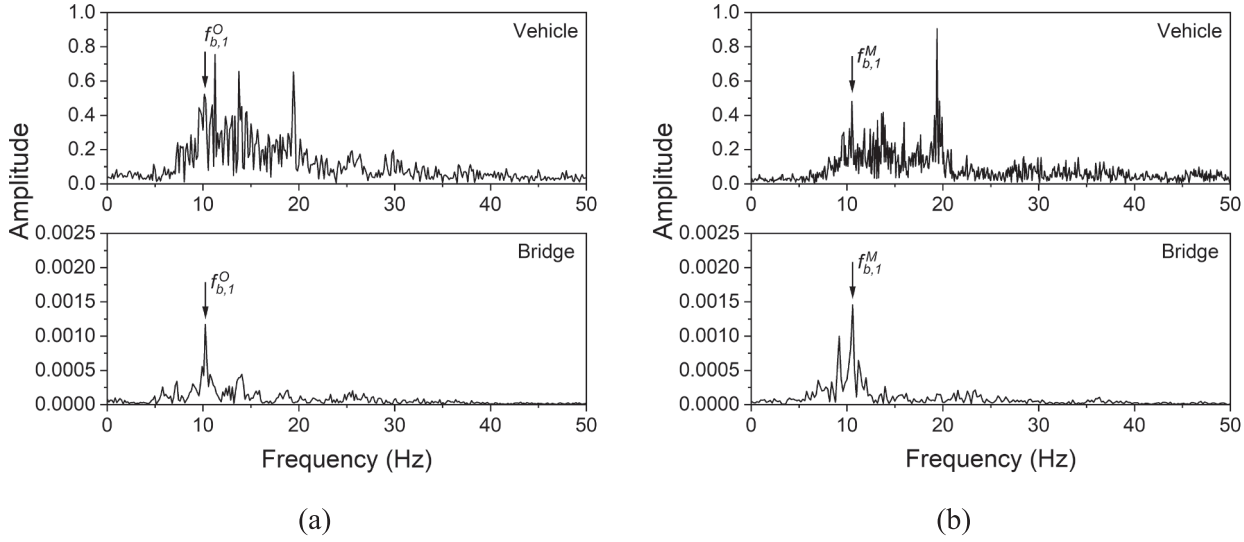

Fig. 19. FFT results: (a) Olari bridge, (b) Matti bridge.

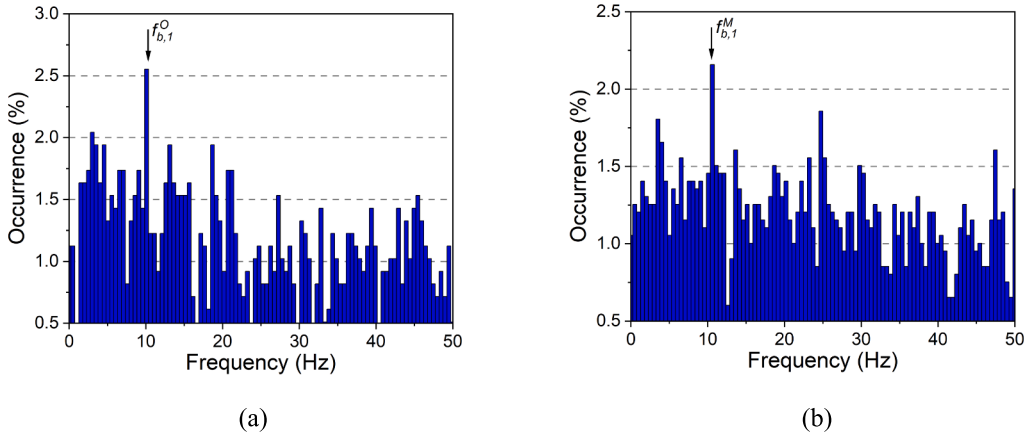

Fig. 20. Distribution of PPs: (a) Olari bridge, (b) Matti bridge.

Table 6
Indexes for two bridges.

	PI	*CV*	*CI*
Olari bridge	1.53	0.21	7.29
Matti bridge	1.80	0.22	8.19

(2) Based on the numerical results, the effect of road roughness, which is one of the most critical factors affecting drive-by methods, was eliminated. Interestingly, poor road conditions did not degrade the performance of the proposed algorithm in frequency recognition, and the algorithm was not affected by roughness levels.
(3) The frequency identified by the algorithm was a statistical result, and a larger number of measurements could improve the clarity of the results and ensure reliable frequency estimation. This encourages the use of more measurements in engineering practice.
(4) Monte Carlo simulations demonstrated the effectiveness of the proposed algorithm and validated that the algorithm was not affected by variations in vehicle parameters, including speed and mass, during different runs. This is particularly advantageous for long-term vehicle-based bridge monitoring, where vehicle parameters may change.
(5) Instead of attempting to minimize differences, this approach encourages the introduction of variability in drive-by measurements (e.g., varying vehicle parameters and avoiding passing the same road surface) to effectively filter bridge frequency, making it particularly attractive in engineering practice.
(6) Field tests performed on city buses validated the feasibility of bridge frequency identification using the proposed algorithm for engineering applications.

Despite the findings summarized above, further investigation is required to assess the applicability of this method to a broader range of bridge and vehicle types. Some simulation results require further experimental validation. Moreover, the current numerical study is based on a 2-DOF quarter-car model to simulate the rear axle system of a bus, and does not represent a full bus system. Future studies should consider models with higher DOFs. The frontier of this study is the application of the proposed algorithm to crowd-sensing vehicle monitoring. This involves using measurements from multiple buses to establish a public-transport-based networked urban bridge monitoring system. Monitoring railway bridges using multi-carriage trains is another avenue of exploration.

CRediT authorship contribution statement

Yifu Lan: Conceptualization, Software, Investigation, Formal analysis, Methodology, Writing – original draft. **Zhenkun Li:** Software, Investigation, Writing – review & editing. **Keijo Koski:** Investigation, Data curation, Writing – review & editing. **Ludovic Fülöp:** Investigation, Data curation, Funding acquisition, Project administration, Writing – review & editing. **Timo Tirkkonen:** Investigation, Resources, Writing – review & editing. **Weiwei Lin:** Investigation, Funding acquisition, Supervision, Project administration, Writing – review & editing.

Declaration of Competing Interest

The authors declare that they have no known competing financial interests or personal relationships that could have appeared to influence the work reported in this paper.

Data availability

The test data is owned by the Finnish Transport Infrastructure Agency (FTIA), and reasonable requests can be sent directly to FTIA.

Acknowledgement

This research is sponsored by the Jane and Aatos Erkko Foundation in Finland (Grant No. 210018). Yifu Lan is also financially supported by the Finnish Foundation for Technology Promotion (TES) and Chinese Scholarship Council (CSC). The bridge measurement data was collected in the SILKUNSE project (Contract Nr. 118951), within the "Digitalisaatiohankkeesta 2016-2018" program of the Finnish Transport Infrastructure Agency (FTIA). The continuous support and inspiration for developing a vehicle-based bridge monitoring system in Finland of Prof. Miyamoto from Yamaguchi University (Japan) and Dr. Yabe from KOZO KEIKAKU Engineering Inc. (Japan) are gratefully acknowledged.

References

[1] Nagayama T, Reksowardojo AP, Su D, Mizutani T. Bridge natural frequency estimation by extracting the common vibration component from the responses of two vehicles. Eng Struct 2017;150:821–9. https://doi.org/10.1016/j.engstruct.2017.07.040.
[2] Farrar C, Hemez F, Shunk D, Stinemates D, Nadler B. A review of structural health monitoring literature: 1996–2001; 2004.
[3] Abdulkarem M, Samsudin K, Rokhani FZ, A Rasid MF. Wireless sensor network for structural health monitoring: a contemporary review of technologies, challenges, and future direction. Struct Health Monitor 2020;19:693–735. https://doi.org/10.1177/1475921719854528.
[4] Malekjafarian A, McGetrick PJ, E.J., OBrien. A review of indirect bridge monitoring using passing vehicles. Shock Vib 2015;2015. https://doi.org/10.1155/2015/286139.
[5] Yang YB, Lin CW, Yau JD. Extracting bridge frequencies from the dynamic response of a passing vehicle. J Sound Vib 2004;272:471–93. https://doi.org/10.1016/S0022-460X(03)00378-X.
[6] Makki Alamdari M, Chang KC, Kim CW, Kildashti K, Kalhori H. Transmissibility performance assessment for drive-by bridge inspection. Eng Struct 2021;242:112485. https://doi.org/10.1016/j.engstruct.2021.112485.
[7] Lan Y, Zhang Y, Lin W. Diagnosis algorithms for indirect bridge health monitoring via an optimized AdaBoost-linear SVM. Eng Struct 2023;275:115239. https://doi.org/10.1016/j.engstruct.2022.115239.
[8] Yang YB, Yang JP. State-of-the-art review on modal identification and damage detection of bridges by moving test vehicles. Int J Struct Stab Dyn 2018;18:1850025. https://doi.org/10.1142/S0219455418500256.
[9] Miyamoto A, Puttonen J, Yabe A. Long term application of a vehicle-based health monitoring system to short and medium span bridges and damage detection sensitivity. Engineering 2017;9:68–122. https://doi.org/10.4236/eng.2017.92005.
[10] Koski K, Fülöp L, Tirkkonen T, Yabe A, Miyamoto A. Heavy vehicle-based bridge health monitoring system. Bridge Maintenance, Safety, Management, Life-Cycle Sustainability and Innovations, CRC Press; 2021. 10.1201/9780429279119-48.
[11] Miyamoto A, Yabe A. Development of practical health monitoring system for short- and medium-span bridges based on vibration responses of city bus. J Civ Struct Heal Monit 2012;2:47–63. https://doi.org/10.1007/s13349-012-0017-0.
[12] Malekjafarian A, Corbally R, Gong W. A review of mobile sensing of bridges using moving vehicles: progress to date, challenges and future trends. Structures 2022;44:1466–89. https://doi.org/10.1016/j.istruc.2022.08.075.
[13] Liu C, Zhu Y, Ye H. Bridge frequency identification based on relative displacement of axle and contact point using tire pressure monitoring. Mech Syst Sig Process 2023;183:109613. https://doi.org/10.1016/j.ymssp.2022.109613.
[14] Wang H, Nagayama T, Nakasuka J, Zhao B, Su D. Extraction of bridge fundamental frequency from estimated vehicle excitation through a particle filter approach. J Sound Vib 2018;428:44–58. https://doi.org/10.1016/j.jsv.2018.04.030.
[15] Yang YB, Mo XQ, Shi K, Wang ZL, Xu H, Wu YT. Contact residue for simultaneous removal of vehicle's frequency and surface roughness in scanning bridge frequencies using two connected vehicles. Int J Str Stab Dyn 2021;21:2171006. https://doi.org/10.1142/S0219455421710061.
[16] Yang YB, Xu H, Zhang B, Xiong F, Wang ZL. Measuring bridge frequencies by a test vehicle in non-moving and moving states. Eng Struct 2020;203:109859. https://doi.org/10.1016/j.engstruct.2019.109859.
[17] Yang YB, Huang CC, Xu H, Wang MH, Wang ZL, Shi K. Frequency extraction for bridges with rough surface by a moving test vehicle enhanced by a shaker. Eng Struct 2022;266:114598. https://doi.org/10.1016/j.engstruct.2022.114598.
[18] Lan Y, Lin W, Zhang Y. Bridge frequency identification using vibration responses from sensors on a passing vehicle. Bridge Safety, Maintenance, Management, Life-Cycle, Resilience and Sustainability, CRC Press; 2022. 10.1201/9781003322641.
[19] Lan Y, Lin W, Zhang Y. Bridge frequency identification using multiple sensor responses of an ordinary vehicle. Int J Struct Stab Dyn 2022::2350056. https://doi.org/10.1142/S0219455423500566.
[20] Bendat JS, Piersol AG. Random data: analysis and measurement procedures. John Wiley & Sons; 2011.
[21] Bernardo JM, Smith AF. Bayesian theory, vol. 405. John Wiley & Sons; 2009.
[22] Z.Mooney C. Monte Carlo simulation. SAGE Publications, Inc.; 1997. 10.4135/9781412985116.
[23] Brady SP, O'Brien EJ, Žnidarič A. Effect of vehicle velocity on the dynamic amplification of a vehicle crossing a simply supported bridge. J Bridg Eng 2006;11(2):241–9.
[24] Yang YB, Lin CW. Vehicle–bridge interaction dynamics and potential applications. J Sound Vib 2005;284:205–26. https://doi.org/10.1016/j.jsv.2004.06.032.
[25] Seetapan P, Chucheepsakul S. Dynamic responses of a two-span beam subjected to high speed 2DOF sprung vehicles. Int J Struct Stab Dyn 2006;6:413–30. https://doi.org/10.1142/S0219455406002015.
[26] Keenahan J, OBrien EJ, McGetrick PJ, Gonzalez A. The use of a dynamic truck–trailer drive-by system to monitor bridge damping. Struct Health Monit 2014;13(2):143–57.
[27] Xu H, Liu YH, Wang ZL, Shi K, Zhang B, Yang YB. General contact response of single-axle two-mass test vehicles for scanning bridge frequencies considering suspension effect. Eng Struct 2022;270:114880. https://doi.org/10.1016/j.engstruct.2022.114880.
[28] Li Z, Lan Y, Lin W. Indirect damage detection for bridges using sensing and temporarily parked vehicles. Eng Struct 2023;291:116459. https://doi.org/10.1016/j.engstruct.2023.116459.
[29] Lin CW, Yang YB. Use of a passing vehicle to scan the fundamental bridge frequencies: an experimental verification. Eng Struct 2005;27:1865–78. https://doi.org/10.1016/j.engstruct.2005.06.016.
[30] Múčka P. Simulated road profiles according to ISO 8608 in vibration analysis. J Test Eval 2018;46:20160265. https://doi.org/10.1520/JTE20160265.
[31] Yang YB, Lee YC, Chang KC. Effect of road surface roughness on extraction of bridge frequencies by moving vehicle. In: Belyaev AK, Irschik H, Krommer M, editors. Mechanics and model-based control of advanced engineering systems. Vienna: Springer; 2014. p. 295–305. https://doi.org/10.1007/978-3-7091-1571-8_32.
[32] Hou J, Li Z, Zhang Q, Jankowski Ł, Zhang H. Local mass addition and data fusion for structural damage identification using approximate models. Int J Struct Stab Dyn 2020;20:2050124. https://doi.org/10.1142/S0219455420501242.
[33] Factors Influencing Bus System Efficiency / Vehicle Size and Type n.d. https://ppiaf.org/sites/ppiaf.org/files/documents/toolkits/UrbanBusToolkit/assets/1/1d/1d8.html [accessed March 24, 2023].
[34] Grafarend EW. Linear and nonlinear models: fixed effects, random effects, and mixed models. Berlin; New York: Walter de Gruyter; 2006.
[35] Li J, Zhu X, Law S, Samali B. Time-varying characteristics of bridges under the passage of vehicles using synchroextracting transform. Mech Syst Sig Process 2020;140:106727. https://doi.org/10.1016/j.ymssp.2020.106727.
[36] Sarwar MZ, Cantero D. Deep autoencoder architecture for bridge damage assessment using responses from several vehicles. Eng Struct 2021;246:113064. https://doi.org/10.1016/j.engstruct.2021.113064.
[37] Shirzad-Ghaleroudkhani N, Mei Q, Gül M. Frequency identification of bridges using smartphones on vehicles with variable features. J Bridg Eng 2020;25:04020041. https://doi.org/10.1061/(ASCE)BE.1943-5592.0001565.